Development of Stochastic IMU Error Models for INS/GNSS Integration

Elisa Gallon, *Illinois Institute of Technology*

Mathieu Joerger, *Virginia Tech*

Boris Pervan, *Illinois Institute of Technology*

BIOGRAPHY

Elisa Gallon received her bachelor's degree in Mathematics from Universite Blaise Pascal, France in 2014 and her Master of Science in Global Navigation Satellite Systems from ENAC and ISAE-Supaero in 2016. From 2016 to 2017, she worked at the European Space Agency (ESA) on Orbit Determination and Time Synchronization of Galileo satellites. She is currently a Ph.D. Candidate at the Navigation Laboratory in the Department of Mechanical and Aerospace Engineering at Illinois Institute of Technology (IIT) in Chicago.

Mathieu Joerger obtained a Master in Mechatronics from the National Institute of Applied Sciences in Strasbourg, France, in 2002. He earned a M.S. in 2002 and a Ph.D. in 2009 in Mechanical and Aerospace Engineering at IIT in Chicago. He is the 2009 recipient of the Institute of Navigation (ION) Bradford Parkinson award, and the 2014 recipient of the (ION) Early Achievement Award. He is also an Associate Editor of Navigation for the Institute of Electrical and Electronics Engineers (IEEE) Transactions on Aerospace and Electronic Systems. Dr. Joerger is currently assistant professor at Virginia Tech, in Blacksburg, VA, working on multi-sensor integration for safe navigation and collision warning of automated driving systems (ADS). He is a member of the E.U./U.S. Advanced RAIM (ARAIM) Working Group C.

Boris Pervan is a Professor of Mechanical and Aerospace Engineering at IIT, where he conducts research on advanced navigation systems. Prior to joining the faculty at IIT, he was a spacecraft mission analyst at Hughes Aircraft Company (now Boeing) and a postdoctoral research associate at Stanford University. Prof. Pervan received his B.S. from the University of Notre Dame, M.S. from the California Institute of Technology, and Ph.D. from Stanford University. He is an Associate Fellow of the AIAA, a Fellow of the Institute of Navigation (ION), and Editor-in-Chief of the ION journal NAVIGATION. He was the recipient of the IIT Sigma Xi Excellence in University Research Award (2011, 2002), Ralph Barnett Mechanical and Aerospace Dept. Outstanding Teaching Award (2009, 2002), Mechanical and Aerospace Dept. Excellence in Research Award (2007), University Excellence in Teaching Award (2005), IEEE Aerospace and Electronic Systems Society M. Barry Carlton Award (1999), RTCA William E. Jackson Award (1996), Guggenheim Fellowship (Caltech 1987), and Albert J. Zahm Prize in Aeronautics (Notre Dame 1986).

ABSTRACT

In this paper, we develop, implement, and test a new high-integrity frequency-domain measurement error modeling method for inertial measurement units (IMU). The IMU error modeling method is intended for safety-critical navigation applications. The method uses both the Allan Variance to identify individual IMU error components and the Power Spectral Density (PSD) to derive a bounding error time-correlation model. By upper-bounding the sample PSD of individual IMU error components, we can guarantee a bound on the state estimation error variance. The method is applied using experimental data from a tactical grade IMU.

I. INTRODUCTION

Global Navigation Satellite Systems (GNSS) can provide continuous worldwide absolute positioning but require visibility of four or more satellites, which is not always achievable in sky-obstructed environments. Also, GNSS are vulnerable to radio-frequency interference. In contrast, inertial sensors are not directly impacted by these external factors. Inertial Navigation Systems (INS) can be used as dead reckoning sensors to estimate displacements over time, but state estimation errors drift due to the temporal integration of IMU errors. Combining INS and GNSS, for example using a Kalman filter (KF), can simultaneously limit the drift in INS positioning error and provide continuity through sky obstructions and robustness against GNSS jamming and spoofing attacks [1]. GNSS/INS integration relies on filtering measurements over time, which requires robust modeling of stochastic errors over time to ensure navigation integrity.

Analytical integrity risk bounds for time-sequential linear estimators can be derived using autocorrelation function (ACF) bounding [2]. This approach requires continuous, cumulative storage of all data and estimator coefficients over time, and except

34th International Technical Meeting of the Satellite Division of the Institute of Navigation (ION GNSS+ 2021), September 20-24, 2021

2565

https://doi.org/10.33012/2021.17962

for short, finite-horizon intervals, is unsuitable for KF implementations. The PSD bounding method, unlike ACF bounding, is not restricted to fixed-interval implementations and is compatible with Kalman filtering [2]. In prior work, we derived high-integrity models for GNSS errors with uncertain time correlation, including satellite orbit and clock ephemeris errors and tropospheric delays [3,4]. But IMU errors remain unaddressed.

In this paper, we develop a methodology to model IMU errors over time using PSD bounding. We identify and bound individual IMU error components for consistency with prior work and with manufacturer specifications. We implement the method using experimental data. IMU errors can be modeled as a sum of independent error components [5]. These elements of gyroscope and accelerometer errors can be analyzed using the Allan Variance (AV) [5–7]. The AV is a time-domain representation originally derived to study the stability of oscillators. It is often adopted by IMU manufacturers because it allows for the identification of the different components of the IMU errors. The AV σ_y^2 of a process y, is related to its PSD S_y by the following equation ([8]):

$$\sigma_y^2(\tau) = 2 \int_0^\infty \frac{\sin^4(\pi f \tau)}{(\pi \tau f)^2} S_y(f) df \tag{1}$$

In practice, computation of the AV is done using clusters of data within the sampled record of raw sensor measurements. Depending on how small these clusters are (i.e., how many data points are involved), the AV can identify each noise term affecting the sensor, making it a very useful approach for manufacturers. Generally, the mapping from σ_y^2 to S_y described in Equation 1 is not one-to-one (as demonstrated in [9]), meaning that a single AV representation can have multiple corresponding PSD curves. Most of the error components used to model the INS errors do have a one-to-one mapping between the AV and PSD domains (as will be shown in Section II), but spectral ambiguity may remain for at least one error source (bias instability).

The work in [2] developed an approach to robust error modeling, through PSD bounding, to ensure KF output integrity. No such guarantees are available in the AV domain, and models based solely on AVs of IMU errors cannot guarantee estimation integrity. Therefore, we employ the PSD bounding approach ([2,4]).

In the first part of this paper, we present a methodology to model IMU errors using PSDs. IMU specifications are reviewed and dominant parameters are selected and converted to the PSD domain. Manufacturer specs are used as the starting point and are then inflated until the model PSDs upper bound the empirical PSDs at all frequencies. The inflated specs are then used as our final model parameters.

The second part of the paper applies this methodology to an example sensor. Following the procedure detailed in the first part of the paper, the error data from accelerometers and gyroscopes is analyzed in the frequency domain and used to generate a high-integrity IMU model. We conclude the paper by comparing our robust error model to the IMU's manufacturer spec sheet.

II. METHODOLOGY

1. IMU error model structure

IMU errors are complex stochastic processes that can be modeled differently depending on the application of interest. For high-precision navigation applications, or applications involving long periods of time without external aiding, comprehensive error models are needed. Such models must include the effects of acceleration sensitivity errors, cross-axis sensitivity errors, non-orthogonality errors and installation misalignment errors [10]. In this work, we are primarily interested in inertial-$aided$ applications and will therefore restrict ourselves to an error model structure widely-used for this purpose ([1,5–7,11]),

$$q_m = (1 + s_f)q_t + b(t) + p(t) + \nu_s(t) \tag{2}$$

where q_m is the measured output, which can be that of an accelerometer or gyroscope. The true value of the variable being measured q_t is impacted by a scale factor error s_f, a time-varying bias b, an acceleration/rate random walk (Ac/R-RW) p, and a velocity/angular random walk (V/An-RW) ν_s for an accelerometer/gyro, respectively.

When a noisy sensor output signal is integrated, the result drifts over time due to the accumulation of the noise. This drift is called random walk. For IMU errors, there are two types of random walks: the angular random walk for gyroscopes, and the velocity random walk for accelerometers. The V/An-RW component is due to thermo-mechanical fluctuations within the sensor and is modeled as additive white Gaussian noise with zero mean.

IMU sensors can also be impacted by an acceleration RW (for accelerometers) or a rate RW (for gyroscopes). In the rest of this paper, this term will be called Ac/R-RW. Their time derivatives can be modeled as:

$$\dot{p}(t) = \nu_p(t) \tag{3}$$

where $\nu_p(t)$ is a white Gaussian process, with zero mean and standard deviation σ_p.

The bias component can be expressed as:

$$b(t) = b_r + b_s(t) \tag{4}$$

The initial bias of an IMU will be different at each power-up due to signal processing initial conditions and physical properties (thermal, mechanical, and electrical variations). This random variation in initial bias is known as the turn-on bias stability (or bias repeatability) b_r.

The bias stability (or bias instability) b_s is the time-varying component of the bias and measures how much deviation or drift the sensor experiences from its starting value. It is a measure of how stable the bias is over a given time period under constant temperature.
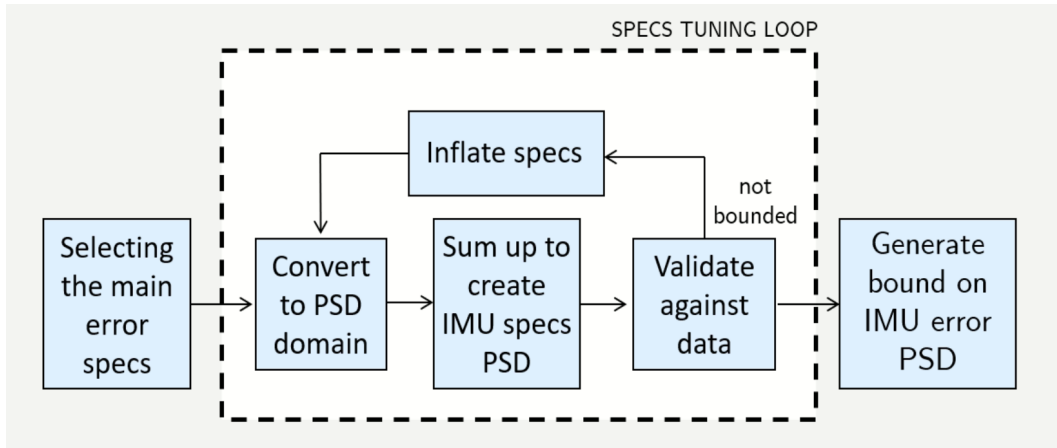
Figure 1 Overview of IMU modeling methodology

2. Modeling of IMU errors components

We evaluate individual manufacturer IMU specifications by measuring their corresponding error components and upper-bounding them in the PSD domain (e.g. white noise + GMRP + Ac/R-RW). The methodology of this work is captured in Figure 1. We selected the 5 IMU parameters listed in Table 1. These IMU error parameters are recurring in manufacturer spec sheets and account for the most dominant sources of errors.

Parameters	Accelerometer units	Gyroscope units
Bias repeatability, σ_{b_r} (1-sigma)	mg	deg/hr
Bias instability, σ_{b_s} (1-sigma)	mg	deg/hr
Scale Factor Accuracy, s_f	ppm	ppm
Velocity/Angular Random Walk, N_0	m/s/$\sqrt{\text{hr}}$	deg/$\sqrt{\text{hr}}$
Acceleration/Rate Random Walk, K	m/s/hr$^{3/2}$	deg/hr$^{3/2}$

Table 1 IMU model parameters selected for evaluation

For IMUs that do not compensate internally for vibrations or temperature changes, parameters that account for these effects should be added to Table 1. The following subsections describe how to interpret each of these components in the PSD domain. To help with those interpretations, Figure 2 shows a representation of inertial error components which can be identified by their distinct linear behavior in Allan variance plots.

a. Bias repeatability

The bias repeatability can be perceived as an initial bias on the IMU errors. The constant value of this initial bias is modeled as following a zero-mean Gaussian distribution with standard deviation σ_{b_r}. Because the mean is removed prior to PSD estimation, this term has no impact on the PSD bounding process.

b. Bias (in)stability

Bias (in)stability is a flicker noise. But flicker noise cannot be modeled in the state space domain [12]. Instead, bias (in)stability is modeled as a first order GMP (FOGMP) with standard deviation σ_{b_s} and time constant τ. If σ_{b_s} is very often provided in IMU specs, it is rarely the case for τ. However, the specs usually provide AV plots of the errors, which can be used to find both σ_{b_s} and τ. The bias (in)stability is represented on an AV plot by a zero-slope curve expressed as [8]:

$$\sigma_0^2(\tau) = \frac{2\sigma_{b_s}^2}{\pi}\ln 2. \tag{5}$$

Since $\sqrt{\frac{2\ln 2}{\pi}} \approx 0.664$, σ_{b_s} can be determined from the zero-slope portion of the AV-curve using the following equation:

$$\sigma_{b_s} = \frac{\sigma_0}{0.664}. \tag{6}$$

The approximate time constant τ of the first order GMP can be extracted from the same portion of the AV curve as illustrated in Figure 2. The PSD of a first order GMP can then be expressed as [13]

$$S_{GMP}(f) = \frac{2}{\tau}\frac{\sigma_{b_s}^2}{(2\pi f)^2 + \frac{1}{\tau^2}}. \tag{7}$$

c. Velocity/Angular Random Walk

The random walk component of inertial sensor errors is modeled as white noise with PSD expressed as

$$S_{WN} = \frac{N_0}{2}, \tag{8}$$

where N_0 is the white noise's PSD constant. The random noise of a sensor is specified either in terms of its PSD or in terms of RW (see units in Table 1). The conversion from one to the other is as follows [8]

$$S_{WN} = \left(\frac{RW}{60}\right)^2. \tag{9}$$

The velocity/angular RW is represented in the AV domain as a line of slope $-1/2$ expressed as [8]

$$\sigma_{-1/2}^2(\tau) = \frac{N_0}{\tau}. \tag{10}$$

The value for N_0 can also be read on the AV plot at τ=1 s, as shown in the center chart of Figure 2.

d. Acceleration/Rate Random Walk

Unlike the previous two parameters, Ac/R-RW may not be given in IMU specifications. However, if such a process contributes to sensor error, it will appear in the AV plot as a line with slope $1/2$. The line's equation can be expressed as [8]

$$\sigma_{1/2}^2(\tau) = \frac{K^2\tau}{3}. \tag{11}$$

Parameter K can then be found on the AV plot as the value of $\sigma_{1/2}$ line at τ=3 s. The PSD of the acceleration/rate RW, can then be expressed as

$$S_{Ac/R-RW}(f) = \left(\frac{K}{2\pi f}\right)^2. \tag{12}$$

The total PSD obtained from the IMU specs can be computed by summing Equations 7, 9, and 12:

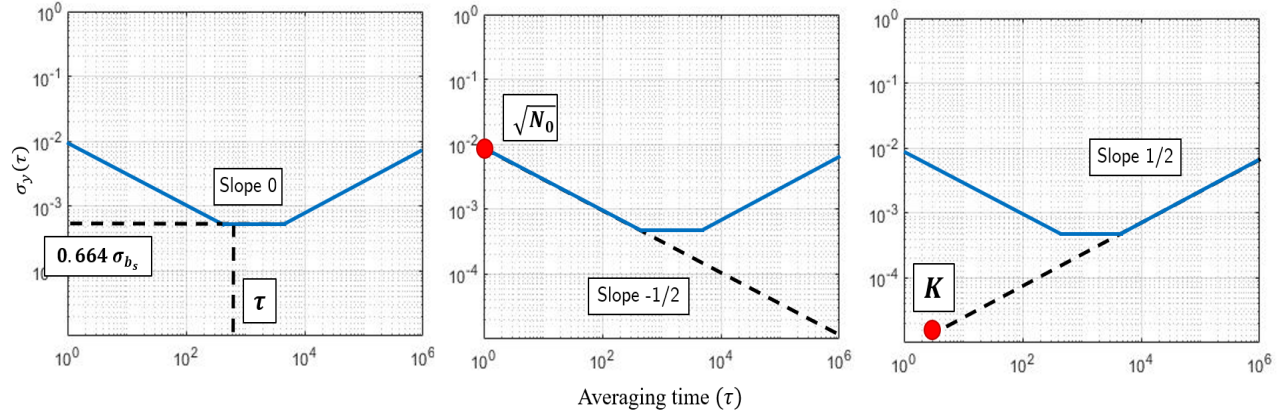$$S_{IMU}(f) = S_{WN}(f) + S_{GMRP}(f) + S_{Ac/R-RW}(f). \tag{13}$$

Figure 2 Extracting model parameters from AV plot

e. Robust error modeling

The total PSD $S_{IMU}(f)$ in Equation 13 the models of its component are obtained using specifications and related information provided by the manufacturer. To ensure estimator integrity, we must validate the models using experimental test data. PSDs of sampled data measure the actual frequency content of the *sum* of all the error sources. They are therefore directly comparable to $S_{IMU}(f)$ in Equation 13. To ensure integrity, the error models actually implemented in the navigation KF must upper bound both the sample and manufacturer-specified PSDs for all f. However, this by itself is not sufficient because the component errors are independent and their PSDs must also be bounded *individually*. In the PSD domain, separating individual error components is challenging. The AV domain however, allows for a clear separation of each error components.

Equation 1 shows that an upper bound in the PSD domain will automatically result in an upper bound of the AV domain. The reverse implication will need further work to be proven: does upper bounding individual components in the AV domain result in an upper bound of their respective PSDs? Reference [9] shows that the inverse mapping of Equation 1 is not always a one-to-one mapping.

In order to implement the inflated error models in a KF, Equation 2 is linearized about the nominal value of each state, denoted below by an asterisk,

$$q_t = \frac{1}{1 + s_f} \left(q_m - b(t) - p(t) - \nu_s(t) \right) \tag{14}$$

$$= h(q_m^*, b^*, p^*, \nu_s^*, s_f^*) + \frac{\delta h}{\delta q_m}\Big|_* (q_m - q_m^*) + \frac{\delta h}{\delta b}\Big|_* (b - b^*) + \frac{\delta h}{\delta p}\Big|_* (p - p^*) + \frac{\delta h}{\delta \nu_s}\Big|_* (\nu_s - \nu_s^*) + \frac{\delta h}{\delta s_f}\Big|_* (s_f - s_f^*) \tag{15}$$

.

Setting $b^* = p^* = \nu_s^* = s_f^* = 0$, we obtain the following linearized model:

$$q_t = q_m - b - p - \nu_s - q_m^* s_f . \tag{16}$$

The final, inflated IMU model parameters can now be used in a GNSS/INS KF. An illustrative state propagation equation for a simplified, single-position-coordinate navigation problem using an accelerometer can be expressed as

$$\begin{bmatrix} \dot{x} \\ \dot{v} \\ \dot{b} \\ \dot{p} \\ \dot{s}_f \end{bmatrix} = \begin{bmatrix} 0 & 1 & 0 & 0 & 0 \\ 0 & 0 & -1 & -1 & -q_m^* \\ 0 & 0 & -1/\tau & 0 & 0 \\ 0 & 0 & 0 & 0 & 0 \\ 0 & 0 & 0 & 0 & 0 \end{bmatrix} \begin{bmatrix} x \\ v \\ b \\ p \\ s_f \end{bmatrix} + \begin{bmatrix} 0 \\ 1 \\ 0 \\ 0 \\ 0 \end{bmatrix} q_m + \begin{bmatrix} 0 \\ -\nu_s \\ \nu_{b_s} \\ \nu_p \\ 0 \end{bmatrix}, \tag{17}$$

where:

- $\nu_s \sim \mathcal{N}(0, \sigma_s^2)$ is the white noise driving VRW,

- $\nu_{b_s} \sim \mathcal{N}(0, \sigma_{b_s}^2)$ is the white noise driving GMP bias (in)stability, and

- $\nu_p \sim \mathcal{N}(0, \sigma_p^2)$ is the white noise driving AcRW with $\sigma_p = K\Delta t$

From a filtering perspective, the presence of the p (Ac/R-RW) in the state vector, which the literature and manufacturers sometimes choose to neglect, increases the number of states by 6 (3 accelerometers and 3 gyroscopes) and may complicate the GNSS/INS integration. Therefore, it may be tempting to use a more conventional model and replace Equation 2 with

$$q_m = (1 + s_f)q_t + b(t) + \nu_s(t)\,, \tag{18}$$

resulting in the simplified system:

$$
\begin{bmatrix} \dot{x} \\ \dot{v} \\ \dot{b} \\ \dot{s_f} \end{bmatrix} =
\begin{bmatrix} 0 & 1 & 0 & 0 \\ 0 & 0 & -1 & -q_m^* \\ 0 & 0 & -1/\tau & 0 \\ 0 & 0 & 0 & 0 \end{bmatrix}
\begin{bmatrix} x \\ v \\ b \\ s_f \end{bmatrix} +
\begin{bmatrix} 0 \\ 1 \\ 0 \\ 0 \end{bmatrix} q_m +
\begin{bmatrix} 0 \\ -\nu_s \\ \nu_{b_s} \\ 0 \end{bmatrix}. \tag{19}
$$

From and integrity perspective, this order reduction is only permissible if the AV of the instrument (accelerometer or gyroscope) does not show evidence of an Ac/R-RW component. In the rest of this paper we will present a methodology to estimate the parameters in the more general model of Equation 17.

III. EXPERIMENTAL EVALUATION

IMU errors are environment-dependent and can vary with factors including temperature, vibrations, and motion. Generating IMU error models that represent multiple possible scenarios requires costly equipment (e.g., temperature chamber, vibration table, rotation table, etc.) and multiple datasets. In this work, we focus on breaking down and modeling IMU performance for one set of static, constant-ambient-temperature data. The same concepts can be used in other testing environments.

In this section, we apply the methodology presented above to IMU data from a Sensonor STIM-300. The STIM-300 is a small, tactical grade, low weight, high performance IMU that contains 3 highly accurate MEMS gyros, 3 high stability accelerometers and 3 inclinometers. The IMU is factory calibrated and compensated over its entire operating temperature range ($-40°$ C to $+85°$ C). More details on this IMU can be found in [14].

1. Data collection setup

Data collection was performed over multiple 10 h-long periods in static conditions at a 125 Hz sampling frequency. To monitor environmental temperature variations and ensure that they did not exceed the variations that can be compensated by the IMU, a temperature sensor was place next to the IMU (see Figure 3). Five of these data sets satisfied the criterion $\Delta T \leq 1°$ C/10 h and were used in the following work.
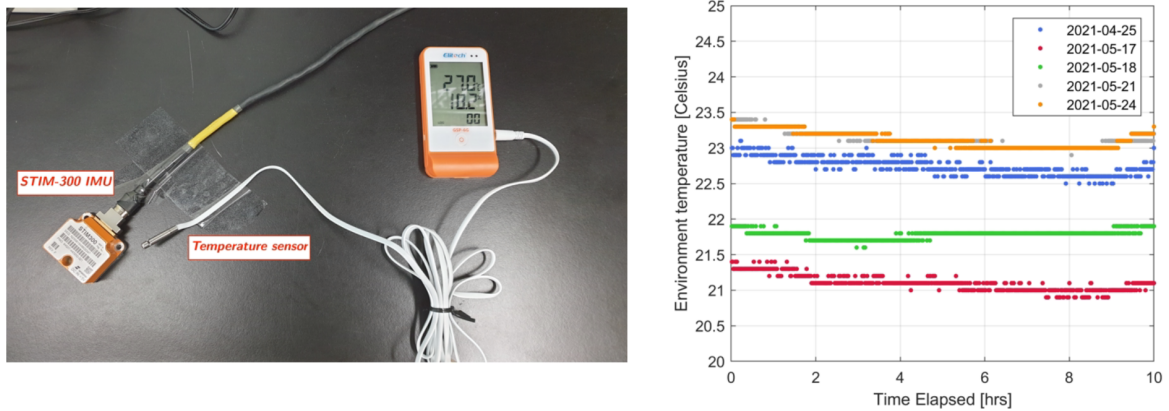

Figure 3 Experimental set up (left) and environment's temperatures (right)
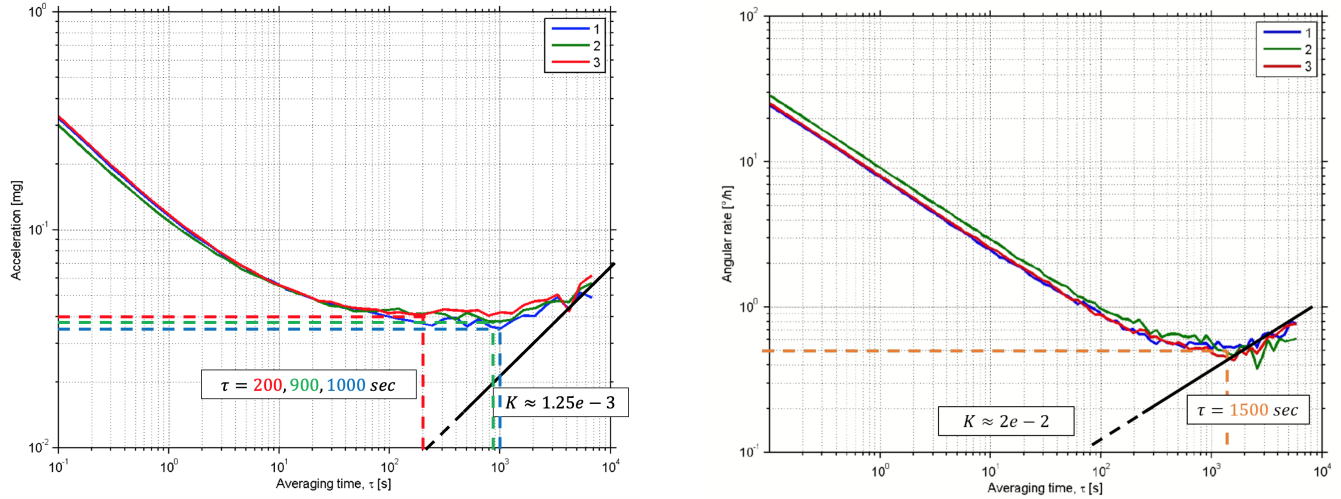
Figure 4 Accelerometer (left) and gyroscope (right) errors Allan Variances provided by the manufacturer's spec from [14]

2. IMU spec conversion to the frequency domain

The STIM-300 IMU spec sheet provides direct values for $\sigma_{b_r}, \sigma_{b_s}, s_f$. The velocity/angular random walk given in the specs can be converted to noise power using Equation 9. AV plots are also provided in the specs, which allow us to determine the values of τ and K.

Figure 4 reproduces the Allan variance plots of the three accelerometers and the three gyroscopes from the STIM-300 spec sheet. First, for the accelerometer, we can see that the three axes seem to have different time constants ranging from 200 sec to 1000 sec. Ideally, this should results in three separate PSD curves in Equations 7 and 13. However, since the reading of τ on the AV plot is subject to ambiguity and since these factors will also be inflated later on, a single, middle value of τ is chosen here. We therefore use a single curve assuming $\tau = 800s$. The acceleration random walk is clearly visible on the AV plot, and its parameter K can be extracted.

The gyroscope errors show that all three axes have similar bias (in)stability time constants of about 1500 sec. All error parameters are summarized in the red columns of Table 2. Their units are the ones described in Table 1.

3. Robust error modeling through PSD bounding

We converted the model derived from the manufacturer specifications to the PSD domain for validation against our sampled data.

A first step to achieve robust modeling of IMU errors is to ensure that they are stationary. To test the data for stationarity, we use a combination of the Levene test and the two-sample Kolmogorov-Smirnov test. The Levene test [15] compares two or more sample populations to determine whether they have equal variance (homoscedastic). The two-sample Kolmogorov-Smirnov test [16] determines whether two samples come from the same distribution. Both tests are performed with a 95% confidence level. If both tests come back positive, the data is considered stationary.

Once stationarity is verified, the data can be used to find an S_{IMU}-model that upper-bounds actual IMU errors at all frequencies. If S_{IMU} obtained using the manufacturer specs fails to provide an upper bound, then these initial model parameter values must be inflated. The process can be iterated until S_{IMU} fully upper-bounds the IMU errors PSD. The impacts of individual parameter inflation on PSD can be found in Appendix A.

We obtained five stationary data sets that are then processed following the methodology in [2] (with windowing parameters $t = 7\,\text{h}$ and $t_s = 10\,\text{h}$) to generate their respective PSD curves. These 15 curves (3 axes and 5 data sets) each for the accelerometers and gyroscopes are represented in grey in Figure 5. Note that to limit the computational cost of generating PSD curve for 10h long datasets at 125 Hz (i.e. 4.5 million points), the data has been re-sampled to 1 Hz (by averaging over 1 sec intervals) prior to PSD estimation (i.e., 36,000 points per curve). This re-sampling will not affect our modeling, since high frequency components are typically not of significant interest for navigation applications. However, higher sample rates can obviously be used if deemed necessary.

For the accelerometers, the red curve represents the PSD curve obtained from the STIM-300 specifications (see Equation 13)
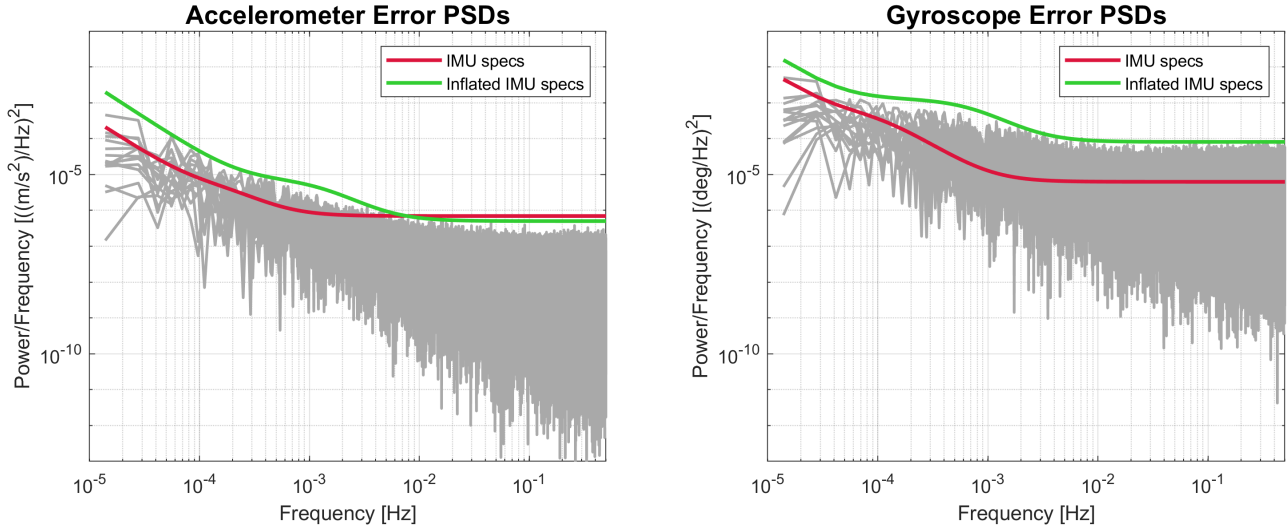
Figure 5 Accelerometer (left) and Gyroscope (right) error PSDs bounding

which are summarized in the red-highlighted columns of Table 3. This red curve represents the data well at high frequencies but not at low frequencies. Based on the conclusions of Appendix A, the white noise component and the GMP time constant were decreased, whereas the GMP standard deviation and the Ac/R-RW were inflated. The final values are listed in the green columns of Table 2 and the final upper-bounding is represented by the green curve of Figure 5. Therefore, the specs are inflated to values described in the green columns of Table 2.

Parameters	Accelerometer	Acc. Inflated	Gyroscope	Gyr. Inflated
σ_{b_s}	0.05	0.165	1.5	5.85
τ	800	120	1500	225
RW	0.05	0.0425	0.15	0.54
K	1.25e-6	3.625e-6	2e-2	3.366e-2

Table 2 Selected IMU specs

A similar approach is performed on the gyroscope errors. In this case, PSD curve obtained from the STIM-300 specifications did not bound the frequency content of the data at any frequency. Therefore, most parameters needed to be inflated (except the GMP time constant, which was decreased). A step-by-step description of specification inflation for the gyroscope errors is described in Appendix A, Section 2.

Note that there is no single model that is uniquely capable of upper bounding the sample PSDs (a different choice of parameters could also work).

Finally, we verify that each error term in Equation 13 is bounded in the AV domain as shown in Figure 6. The inflated parameters provided in Table 3 ensure that each of the error components are upper bounded individually in the AV domain. Both the accelerometer and gyroscope bounds for the V/An-RW and the GMP have a significant margin. However, the gyrsoscope's Ac/R-RW model provides a very tight bound in the AV domain. Note that the bias instabilities are flicker noises, which cannot be modeled in the state space domain. Instead, they are modeled using a FOGMP. The dashed red curves in those figures represent the flicker noises AV upper bound. In order to use a FOGMP, we ensure that this model upper bounds the flicker noise upper bound. Further work will be needed to prove that the bounding in the AV domain of individual errors ensure their bounding in the PSD domain as well, therefore ensuring integrity.

IV. CONCLUSION

In this paper, we developed a new approach to high-integrity inertial error modeling for time-sequential navigation algorithms. The methodology gives an interpretation of the inertial measurement unit (IMU) error components in the frequency domain. For each error component, Allan Variance (AV) and Power Spectral Density (PSD)-domain expressions were derived. Error
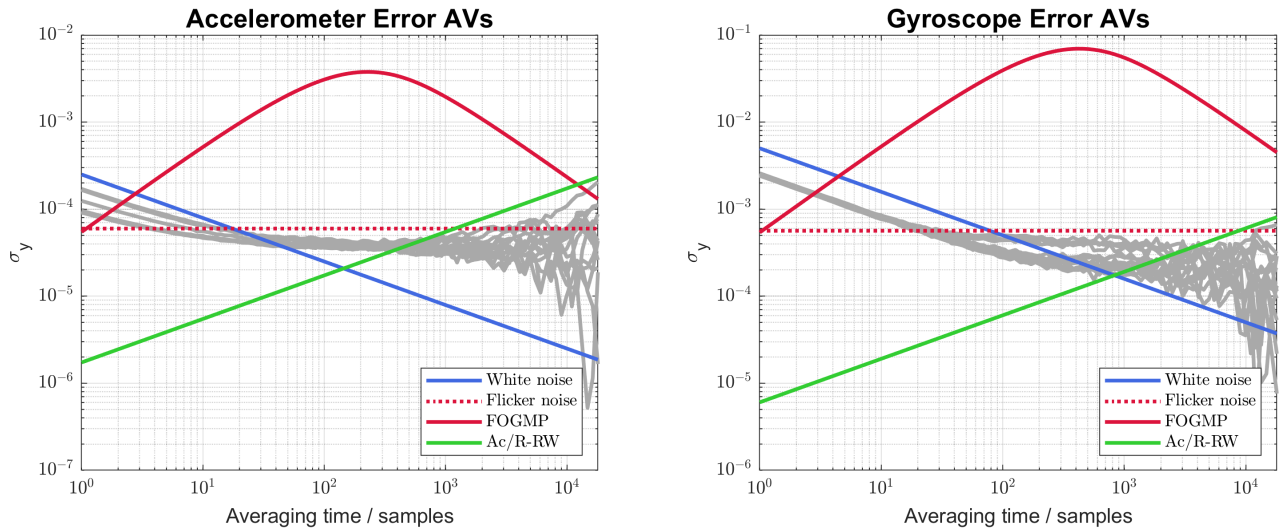
Figure 6 Accelerometer (left) and Gyroscope (right) error AVs bounding

parameters can then be evaluated using information from the IMU specification sheets, and then inflated or deflated to ensure that their PSD is upper bounded.

This methodology was applied to a tactical grade IMU (STIM-300). Overall, we observed that the specifications matched experimental data reasonably well. The PSD curves derived from the specifications needed to be shifted upwards to upper bound the sample errors PSDs. This was achieved by applying inflation factors to the acceleration/rate random walk, the bias (in)stability standard deviation and the white noise. The resulting high-integrity error model was represented in the AV domain: each individual error component was upper bounded in the AV domain.

In future work, we will verify that the upper bounding of individual errors in the AV domain results in their upper bounding in the PSD domain. We will also address the issue of robust modeling of non-stationary errors for large variations in temperature and vibration.

ACKNOWLEDGEMENTS

REFERENCES

[1] C. Tanil, S. Khanafseh, M. Joerger, and B. Pervan, "An INS monitor to detect GNSS spoofers capable of tracking vehicle position," *IEEE Transactions on Aerospace and Electronics*, vol. 64, no. 1, pp. 131–143, 2018.

[2] S. Langel, O. Garcia-Crespillo, and M. Joerger, "A new approach for modeling correlation Gaussian errors using frequency domain ovrebounding," in *Proceedings of the IEEE/ION PLANS 2020*, 2020.

[3] E. Gallon, M. Joerger, and B. Pervan, "Frequency domain modeling of orbit and clock errors for sequential positioning," in *Proceedings of the 33rd International Meeting of the Satellite Division of the Insitute of Navigation (ION GNSS+ 2020)*, 2020.

[4] ——, "Robust modeling of GNSS tropospheric delay dynamics," *IEEE Transactions on Aerospace and Electronic Systems*, 2021.

[5] D. Gebre-Egziabher, "Design and performance analysis of a low-cost aided-dead reckoning navigator," Ph.D. dissertation, Stanford University, 2004.

[6] N. El-Sheimy, H. Hou, and X. Nui, "Analysis and modeling of inertial sensors using allan variance," *IEEE Transactions on Instrumentation and Measurement*, pp. 140–149, 2008.

[7] H. Hou, "Modeling inertial sensors errors using allan variance (master's thesis)," Ph.D. dissertation, University of Calgary, 2004.

[8] "IEEE standard specification format guide and test procedure for single-axis interferometric fiber optic gyros," *IEEE Std*, pp. 1–84, 1999.

[9] C. Greenhall, "Spectral ambiguity of allan variance," *IEEE Transactions on Instrumentation and Measurement*, pp. 623–627, 1998.

[10] D. Titterton and J. Weston, *Strapdown Inertial Navigation Technology*. London, England: Peter Peregrinus Ltd, 1997.

[11] A. Quinchia, G. Falco, F. E., F. Dovis, and C. Ferrer, "A comparison between different error modeling of mems applied to gps/ins integrated systems," *Sensors*, vol. 13, pp. 9549–9588, 2013.

[12] J. A. Farrell, F. O. Silva, F. Rahman, and J. Wendel, "IMU Error State Modeling for State Estimation and Sensor Calibration: A tutorial," *UC Riverside: Bourns College of Engineering*, 2020. [Online]. Available: https://escholarship.org/uc/item/1vf7j52p

[13] C. Chatfield, *The Analysis of Time Series: An Introduction, Sixth Edition*, ser. Chapman & Hall/CRC Texts in Statistical Science. Taylor & Francis, 2003. [Online]. Available: https://books.google.com/books?id=I367jgEACAAJ

[14] Sensonor, "Stim-300 imu product specifications," 2021, accessed: 2021-04-30. [Online]. Available: https://www.sensonor.com/products/inertial-measurement-units/stim300/

[15] H. Levene, "Robust tests for equality of variances," *Contributions to Probability and Satistics: Essays in Honor of Harold Hotelling. Stanford University Press*, pp. 278–292, 1960.

[16] F. Massey, "The Kolmogorov-Smirnov test for goodness of fit," *Journal of the American Statistical Association*, vol. 46, no. 253, pp. 68–78, 1951.

A. IMPACT OF THE IMU SPECS INFLATION ON THEIR POWER SPECTRAL DENSITY

This appendix is divided into two subsections: first, theoretical PSD curves are generated based on specific IMU parameters. Each of these parameters are inflated one-by-one and its effects are observed in the PSD domain. Second, using the knowledge developed in the first subsection, IMU specs are inflated to upper bound the PSD curves of the STIM-300 gyroscope errors described in this paper.

1. Theoretical analysis

Let us go back to the IMU-spec-defined PSD described in Equation 13 as the sum of the PSDs of the various IMU error components: white noise, first order GMP and random walk. Let us now generate one of these curves with the parameters given in Table 3. Note that some of these parameters are larger than the ones typically observed in IMUs. This is to ensure that each of the components of Equation 13 can be distinctly seen on a PSD plot, so as to ensure that the impact of their inflation can be properly observed.

Parameters	Value	Units
Bias instability, σ_{b_s} (1-sigma)	10^{-2}	g
Bias instability, τ	10^3	sec
Velocity/Angular Random Walk, RW	0.1	m/s/$\sqrt{\text{hr}}$
Acceleration/Rate Random Walk, K	10^{-4}	m/s/hr$^{3/2}$
Sampling interval	1	sec
Data length	10	hrs

Table 3 Example IMU specification parameters prior to inflation

The red curves on each plot of Figure 7 represent the output of Equation 13 given the settings described in Table 3. The green curves represent the same equation, provided one of the parameters has been inflated by 50% of its initial value. The orange curves show a similar result, but with a 50% deflation. Figure (a) shows the result of an inflation of the white noise (or velocity random walk). Figure (b) shows an inflation of the acceleration random walk. Figures (c) and (d) show inflation of the standard deviation and time constant (respectively) of the first order GMP.
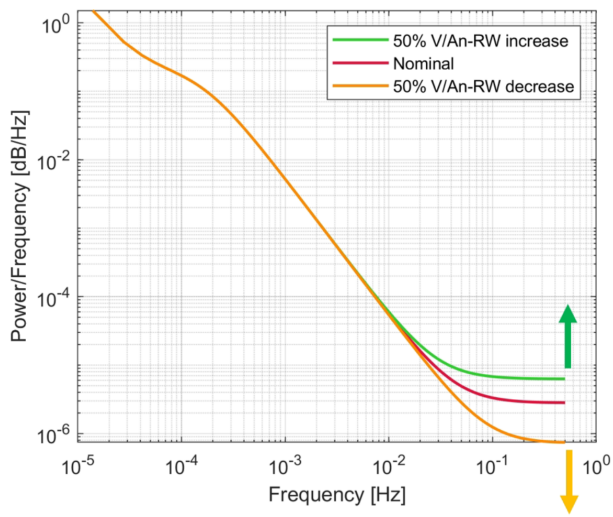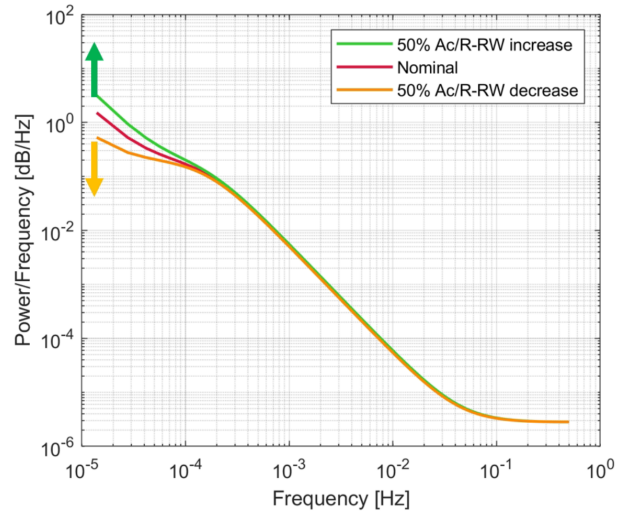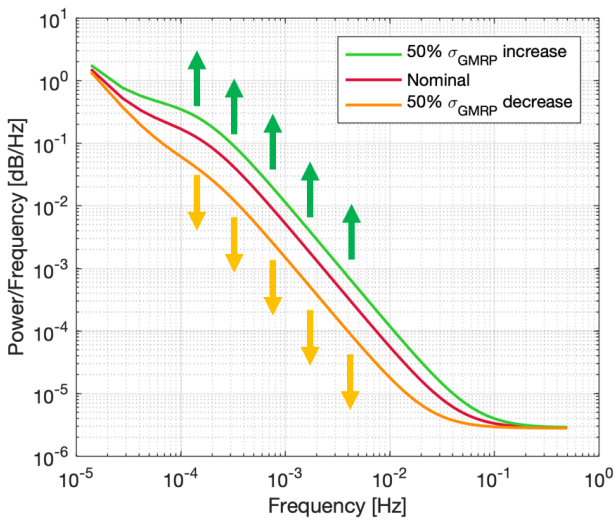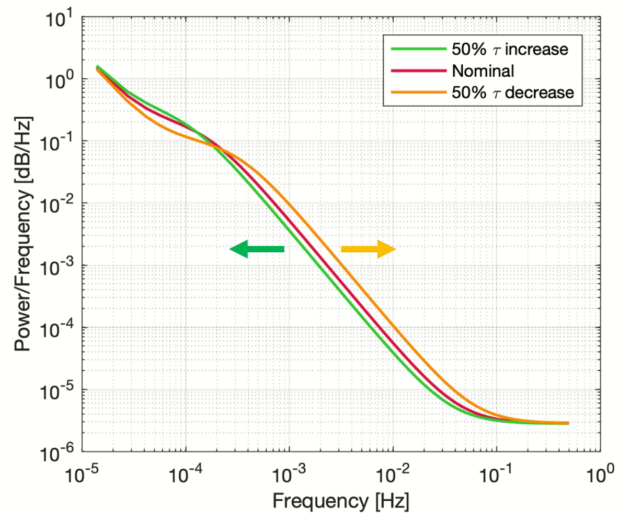
Figure 7 Impact of IMU specs inflation (a-V/An-RW, b-Ac/R-RW, c-GMRP sigma, d-GMRP tau) on theoretical PSD curves

Assuming the PSD upper bounding is prevented by large sample PSD values at low frequencies (right side of the figures), an inflation of the velocity/angle random walk would be recommended. Inflating the V/An-RW would result in an increase of the flat part of the curve at low frequencies.

On the other hand, if the high frequency terms of the sample PSD need to be shifted upwards, inflating the acceleration/rate random walk is recommended, as it will result in an upward shift of the high frequency part of the curve that is characteristic of acceleration random walk PSDs.

To shift the mid-frequency terms of the PSDs upward, an inflation of the standard deviation of the first order GMRP will be needed.

And finally, if the overall shape of the PSD bound needs to be modified, the time constant of the first order GMRP may be inflated or deflated. An inflation will result in a sharper decline in the curve, whereas a deflation of τ will flatten the curve.

2. Application to real data

Now that we know the impact that each IMU specs inflation will have on the overall PSD curve, we can apply that knowledge to a real case (as described in Section III.3): the STIM-300 gyroscope errors.

The red curves in Figure 8 represent the results obtained with the IMU specifications described in the STIM-300 specification sheet [14] and repeated in the red columns of Table 3.

Let us start by inflating the central and left part of the curves. From the previous subsection, we know that the GMP and the Ac/R-RW need to be modified. In Figure (a), inflating σ_{b_s} results in an inflation of the left half of the PSD curve (represented in green). Looking at the grey curve, we can see that the smooth variation in the middle of the plot needs to be dampened: τ has to be deflated, as shown in Figure (b). But the deflation of tau also results in a decrease of the high frequency component (far left of the plot). To upper bound these terms, the Ac/R-RW term K is inflated (as shown in Figure (c)). Finally, only the low frequency components are left to be upper bounded: the V/An-RW term is inflated in Figure (d).

A similar approach can be performed on the accelerometer errors. The final inflated values are described in the green columns of Table 3. Note that the order of inflation and the final values that are chosen here are arbitrary: different sets of values could also result in an acceptable upper-bound.
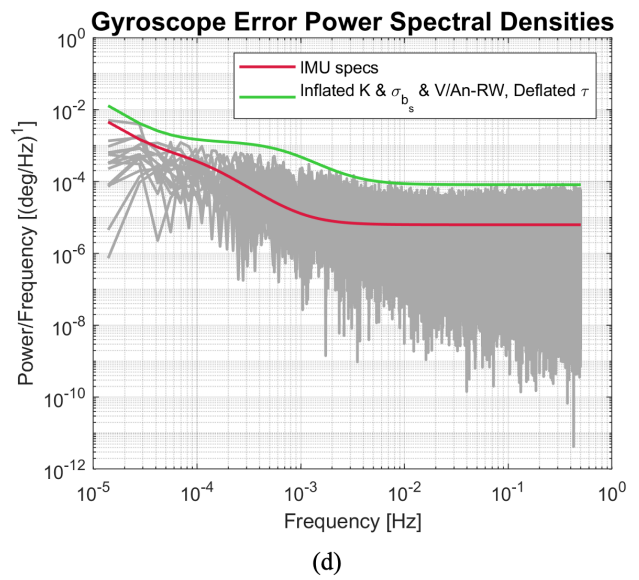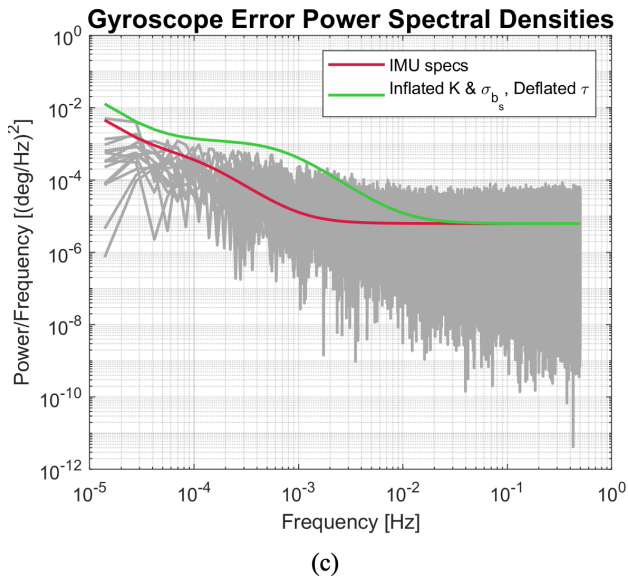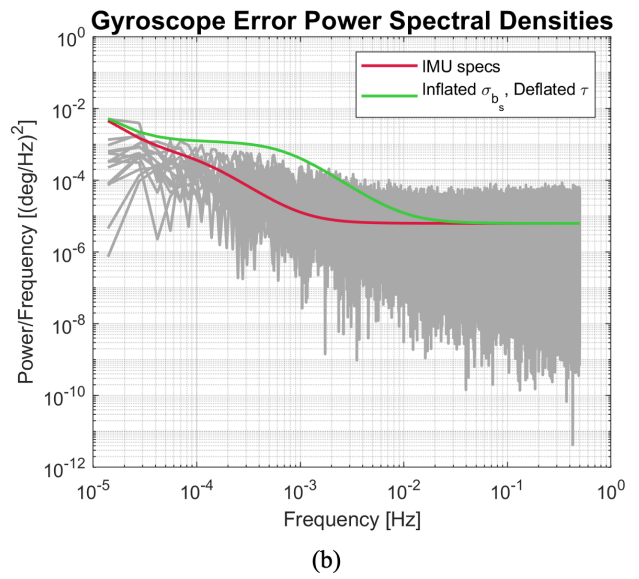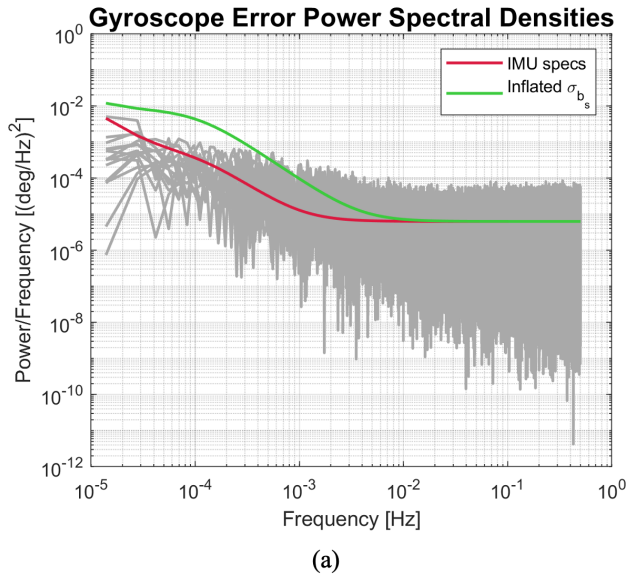
Figure 8 PSD bounding through IMU specs inflation (a-GMP sigma, b-GMP tau, c-V/An-RW, d-Ac/R-RW) on theoretical PSD curves